

VLBA Astrometric Observations of the Cassini Spacecraft at Saturn

Dayton L. Jones

Jet Propulsion Laboratory, California Institute of Technology, Pasadena, CA 91109

dayton.jones@jpl.nasa.gov

Ed Fomalont

National Radio Astronomy Observatory, Charlottesville, VA 22903

Vivek Dhawan

National Radio Astronomy Observatory, Socorro, NM 87801

Jon Romney

National Radio Astronomy Observatory, Socorro, NM 87801

William M. Folkner

Jet Propulsion Laboratory, California Institute of Technology, Pasadena, CA 91109

Gabor Lanyi

Jet Propulsion Laboratory, California Institute of Technology, Pasadena, CA 91109

James Border

Jet Propulsion Laboratory, California Institute of Technology, Pasadena, CA 91109

and

Bob Jacobson

Jet Propulsion Laboratory, California Institute of Technology, Pasadena, CA 91109

ABSTRACT

The planetary ephemeris is an essential tool for interplanetary spacecraft navigation, studies of solar system dynamics (including, for example, barycenter corrections for pulsar timing ephemerides), the prediction of occultations, and tests of general relativity. We are carrying out a series of astrometric VLBI observations of the Cassini spacecraft currently in orbit around Saturn, using the Very Long Baseline Array (VLBA). These

observations provide positions for the center of mass of Saturn in the International Celestial Reference Frame (ICRF) with accuracies ~ 0.3 milli-arcsecond (1.5 nrad), or about 2 km at the average distance of Saturn. This paper reports results from eight observing epochs between 2006 October and 2009 April. These data are combined with two VLBA observations by other investigators in 2004 and a Cassini-based gravitational deflection measurement by Fomalont et al. in 2009 to constrain a new ephemeris (DE 422). The DE 422 post-fit residuals for Saturn with respect to the VLBA data are generally 0.2 mas, but additional observations are needed to improve the positions of all of our phase reference sources to this level. Over time we expect to be able to improve the accuracy of all three coordinates in the Saturn ephemeris (latitude, longitude, and range) by a factor of at least three. This will represent a significant improvement not just in the Saturn ephemeris but also in the link between the inner and outer solar system ephemerides and in the link to the inertial ICRF.

Subject headings: techniques: interferometric — astrometry — planets and satellites: individual (Saturn)

1. Introduction

Planetary ephemerides are used for multiple purposes including dynamical mass determination for solar system bodies, pulsar timing, high-precision tests of general relativity, and inter-planetary spacecraft navigation. During the past several decades a series of increasingly accurate ephemerides have been developed at the Jet Propulsion Laboratory (JPL) by adding new data types such as Very Large Array (VLA) astrometry (Muhleman et al. (1985); Muhleman et al. (1986)), spacecraft tracking (Duxbury & Callahan 1989), and radar range measurements (Campbell et al. 1978) to historical and modern optical observations.

Accurate ephemerides are one of the basic tools of observational astronomy, in the same sense as star catalogs and redshift surveys. They represent a community resource whose value is proportional to their accuracy, and whose accuracy requires regular observational support to maintain and improve. A specific example is the great improvement between timing distances and kinematic distances for pulsars when using the newer DE405 ephemeris (Standish 2004) compared with the older DE200 ephemeris (*e.g.*, Verbiest et al. (2008)).

The orbits of the inner planets are very accurately tied together with the current data set. For example, the angular ephemeris errors for Mars with respect to Earth are typically 0.2 milli-arcsecond (mas) or 1 nrad (IAU 2009). However, the outer planets are not as well tied to the inner planets (or each other) because there have been fewer opportunities to supplement optical observations with high precision spacecraft radio tracking data. The Pioneer and Voyager missions provided essentially single data points during their flybys of the outer planets, and the Galileo mission to Jupiter was severely constrained by the loss of its high gain antenna. This restricted

Galileo downlink signals to a relatively low frequency (2.3 GHz) and a low signal/noise ratio. As a result, VLBI observations of Galileo had accuracies of only ~ 5 -10 mas (Jacobson et al. 1999). Thus, the Cassini mission to Saturn (<http://saturn.jpl.nasa.gov/index.cfm>) is our first opportunity to incorporate high-accuracy data from a spacecraft orbiting an outer planet for an extended period. For reference, an angle of 0.1 mas (0.5 nrad) corresponds to about 750 meters at the average distance of Saturn from Earth.

Our goal is to improve the position of Saturn in the International Celestial Reference Frame (ICRF, see Ma et al. (1998)) through phase-referenced VLBI observations of Cassini using the Very Long Baseline Array (VLBA)¹ at 8.4 GHz (X band) combined with Cassini orbit determinations. The Cassini orbit can be determined to about 2 km at apoapse and 0.1 km at periapse relative to the center of mass of Saturn with range and Doppler tracking by the Deep Space Network (Antreasian et al. 2008). The future Juno mission to Jupiter should allow a similar application of phase-referenced VLBI to improve the Jupiter ephemeris. Combined with our new data for Saturn this will lead to a better model for the gravitational interactions, and the orbital evolution, among all the outer planets. A covariance analysis (Standish 2006) at JPL shows that with only a few years of VLBA data, the ephemeris improvement for Saturn extends for decades.

2. Observations

We have observed Cassini with the VLBA at eight epochs, each typically four hours long, during the past three years. Table 1 lists the dates of each epoch and the VLBA antennas that were used. The VLBA consists of ten radio antennas, each 25 meters in diameter, located at sites from the US Virgin Islands to Hawaii. It has demonstrated an unrivaled astrometric precision of less than 10 micro-arcseconds (μas) in favorable circumstances (e.g., Fomalont & Kopeikin (2003)). The spacecraft's 8 GHz signals provide more than adequate SNR as shown in Figure 1.

¹The VLBA is operated by the National Radio Astronomy Observatory (NRAO).

Table 1. Observing Epochs and VLBA Antennas Used

Epoch	Obs. Date	VLBA Antennas
BJ061A	2006 Oct 11	SC, HN, NL, FD, LA, PT, KP, OV, MK
BJ061B	2007 Mar 1	SC, HN, NL, FD, LA, PT, KP, OV, BR, MK
BJ061C	2007 Jun 7	SC, HN, NL, FD, LA, PT, KP, OV, BR, MK
BJ061D	2008 Jan 12	SC, HN, NL, LA, PT, KP, OV, BR, MK
BJ061E	2008 Jun 13	SC, HN, FD, LA, KP, OV, MK
BJ061F	2008 Aug 1	SC, HN, NL, FD, LA, PT, KP, OV, BR, MK
BJ061G	2008 Nov 11	HN, NL, FD, LA, PT, KP, OV, BR, MK
BJ061H	2009 Apr 24	SC, HN, NL, FD, LA, PT, KP, OV, BR, MK

Note. — The VLBA antenna locations are: SC = St. Croix, US Virgin Islands; HN = Hancock, NH; NL = North Liberty, IA; FD = Fort Davis, TX; LA = Los Alamos, NM; PT = Pie Town, NM; KP = Kitt Peak, AZ; OV = Owens Valley, CA; BR = Brewster, WA; MK = Mauna Kea, HI.

We used standard phase-referencing techniques (Lestrade et al. (1990); Guirado et al. (1997); Guirado et al. (2001); Fomalont (2006)) with rapidly alternating scans between Cassini and angularly nearby reference sources (see Table 2). In addition, we observed several strong sources spread over the sky during each epoch to allow better calibration of the troposphere (Lestrade (2004); Mioduszewski & Kogan (2004)). We did not attempt to improve the phase calibration by employing multiple phase reference sources when possible, as has been demonstrated by Fomalont & Kogan (2005), but this is an option for future observations.

Figure 2 shows the projected baselines for one of our experiments (BJ061A). For some epochs, including this one, the most northerly VLBA antenna site, in Brewster, WA, was not able to participate. This caused a reduction in north-south resolution. Nevertheless, the over-all baseline coverage is good for a low-declination radio source. It is sufficient for unambiguous phase referencing.

The accuracy of the ICRF is approximately 0.02 mas, based on ~ 200 defining sources each with a typical position error of 0.1-0.2 mas. Individual sources may have larger errors at some epochs due to changes in source structure (e.g., Fey et al. (2004); Porcas (2009)), but the imaging capability of the VLBA allows us to detect and correct for such changes. To maximize the accuracy of our link between the Saturn ephemeris and the ICRF we have devoted a separate observing epoch to tying the phase reference sources to 10-20 high-quality ICRF sources. (The results from this epoch will be reported separately.) This reduced our sensitivity to the structure of individual sources. We expect, based on previous experience with phase referenced VLBI (e.g., Lestrade et al. (1999)), that an absolute accuracy of 0.1 mas with respect to the ICRF can be achieved for our calibration sources. Thus, the final combined error of our Cassini positions with respect to the ICRF will be approximately 0.2 mas, consistent with the level of VLBI spacecraft tracking error predicted by Lanyi, Bagri, & Border (2007). Because the linking of our phase reference sources to the grid of ICRF sources is not complete, the current error for Cassini positions in the ICRF is estimated to be 0.3 mas or greater, depending on the specific phase reference source used. One of our phase reference sources has an ICRF position error less than 0.1 mas, while some of the other reference sources have ICRF positions errors several times larger. Future observations to maintain and improve the ICRF catalog will continue to reduce the position errors of these sources.

Calibration, editing, and other data reduction tasks were carried out using the Astronomical Image Processing System (AIPS)². The only exception was the production of total delays for use by JPL software. This required a specific file format, which was created by combining information from AIPS output tables with a program written by E. Fomalont.

The analysis of data from a phase-referenced VLBI experiment involves multiple steps because there are many types of error that must be calibrated and removed from the data (e.g., Lanyi et al. (2005)). The following subsections describe these analysis steps.

²AIPS is provided and supported by the National Radio Astronomy Observatory.

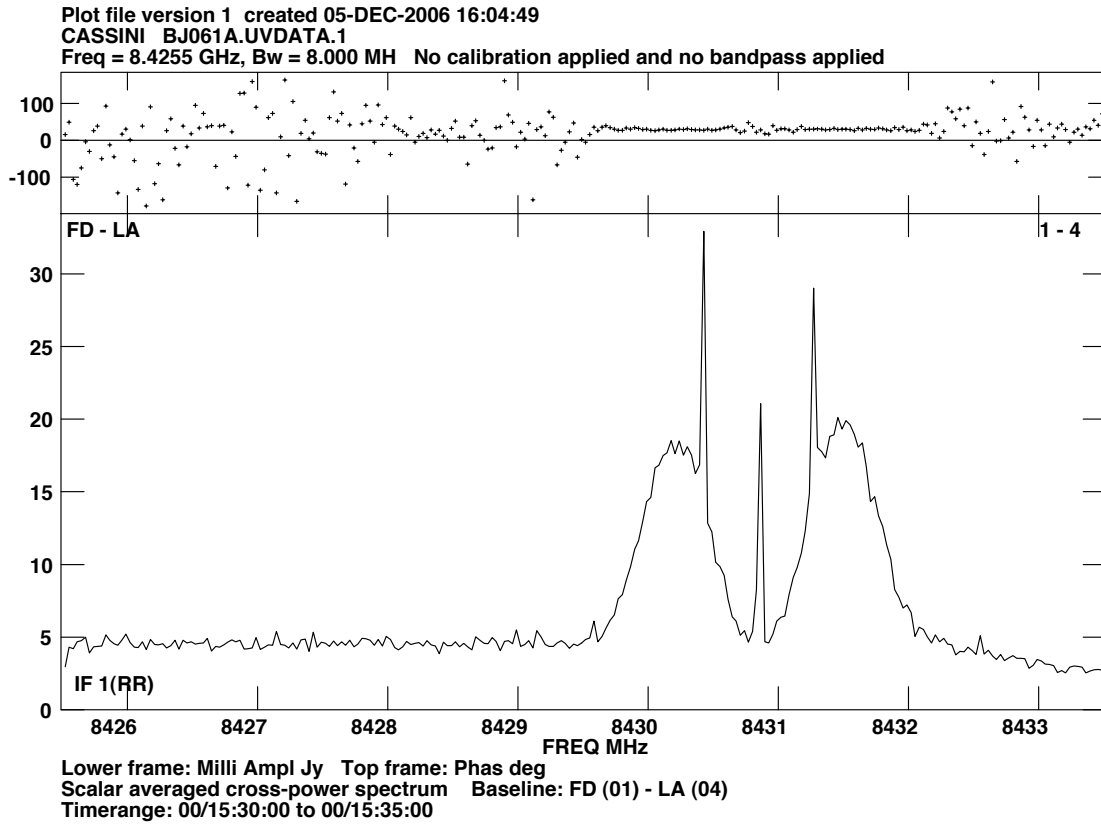


Fig. 1.— Cassini fringe phase (top) and amplitude (bottom) from a single baseline for a typical 1-2 minute scan during our first epoch. The narrow amplitude peaks are the carrier and subcarriers of the spacecraft signal, and the the broad peaks are created by telemetry modulation. The total width of the signal varies with data rate. During this epoch is was approximately 2.5 MHz.

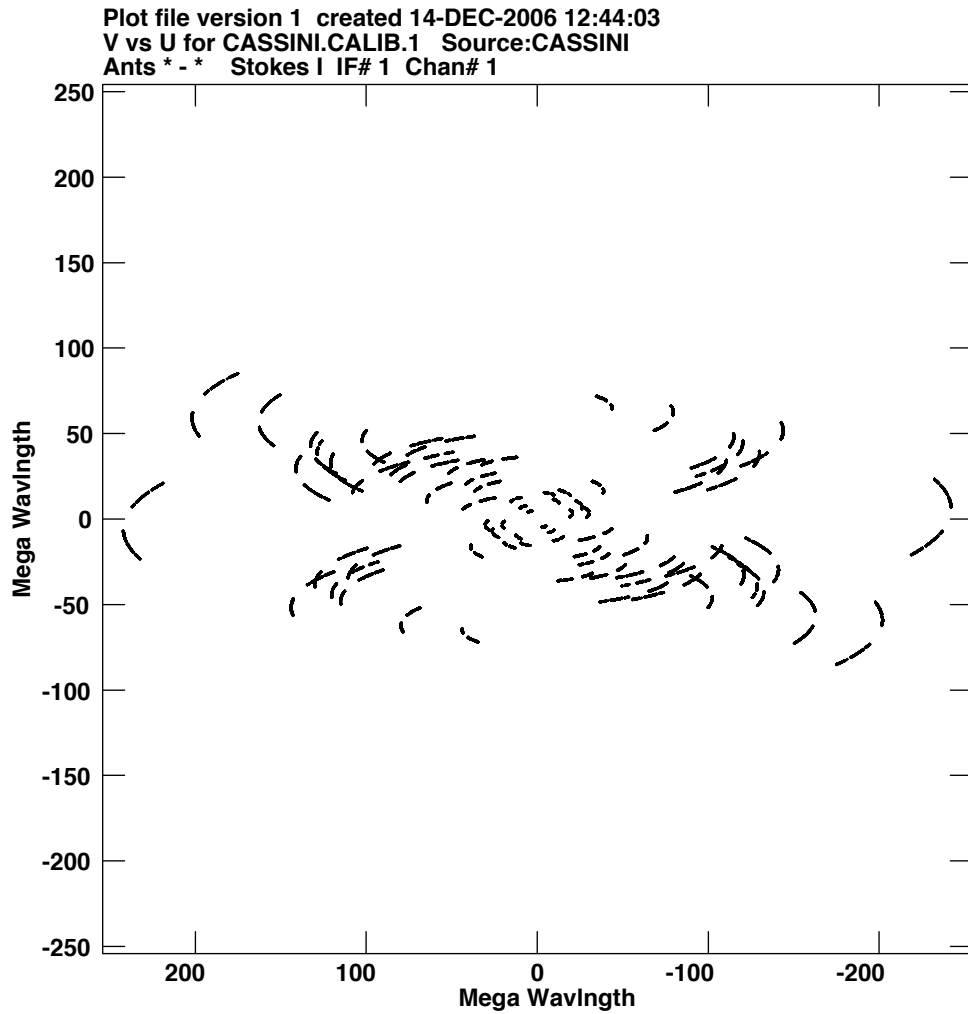


Fig. 2.— (U,V) sampling for Cassini during our first epoch. The sampling for the phase reference source is nearly identical.

3. Experiment Scheduling

There are a number of constraints that must be satisfied when scheduling each epoch. These are:

1. We need to avoid periods near Saturn conjunction with the Sun.
2. Cassini must be transmitting rate telemetry to the Deep Space Network station at Goldstone, CA, at X-band (8.4 GHz).
3. We need to avoid spacecraft trajectory correction maneuvers, moon flybys, and ring occultations.
4. We need a reasonably strong and compact phase reference source within about 2° of Cassini's position.
5. We need to observe multiple strong sources covering a wide range of elevation angles for troposphere calibration during each epoch.

Because Saturn reverses its apparent direction of motion on the sky every year, it is possible with careful scheduling to use the same phase reference source during multiple epochs. This reduces the number of phase reference sources that need to be tied to the ICRF, and minimizes relative errors between epochs due to source structure or ICRF offset differences between difference reference sources.

Note that we did not always have a phase reference source within 2° of Cassini, as desired. There is often a tradeoff between angular separation and reference source flux density, and we did not consider sources with flux densities less than 100 mJy to ensure an adequate signal/noise ratio. In retrospect this flux density cutoff may have been too conservative.

During each observing epoch we alternated scans between Cassini and the phase reference source every 2-3 minutes, and included occasional scans of a strong source for instrumental delay and bandpass calibration. In addition, ~ 10 strong sources covering as wide an elevation range as possible were observed during a 30-40 minute period to allow a zenith troposphere delay to be estimated for each of the VLBA antenna sites.

The data from each epoch were stored prior to correlation until a reconstructed orbit solution for Cassini was available from JPL. The Cassini orbit is determined from Doppler tracking by the Deep Space Network, and provides the *a priori* positions used for Cassini during correlation. Because Cassini transmits in right circular polarization only, we used only the R-R correlator output in our analysis. To avoid decorrelation over time or frequency, and to accurately measure phase across the relatively narrow bandwidth of the Cassini signal, we used 1-second integrations and 256 spectral channels across each 8-MHz IF band.

The four available IF bands were separated in frequency by up to 462 MHz to improve the multi-band delay response. Small changes in the reference frequency were necessary at each epoch to keep the Cassini signal away from the edges of IF band 1. (The frequency of the Cassini signal changes by a few MHz when switching between a one-way downlink and a two-way coherent link.) The center frequencies for each IF band were approximately 8.428, 8.500, 8.790, and 8.890 GHz.

4. Astrometric Position Determinations

4.1. A Priori Calibration

Initial delays were calculated from the geometric model used during correlation (Romney 1999). The *a priori* spacecraft position and proper motion at the start of our observations were corrected, if necessary, from the values used during correlation. (The most accurate Cassini orbit solutions were not available until a few weeks after a particular date.) A subtle but important part of the geometric model is the difference in general relativity corrections for signals propagating through gravitational fields in the solar system, particularly those of the Sun and Saturn. Unlike the phase reference sources, Cassini can not be assumed to be at infinity; only part of the solar system gravitational field applies to signals from Cassini.

Amplitude calibration was based on recorded system temperatures along with previously determined antenna gain curves. Additional amplitude corrections were applied to remove the effect of using two-bit quantization when recording signals at the VLBA antennas. Phases were corrected for parallactic angle and for improvements in the values of Earth orientation parameters (UT1 and

polar motion). Instrumental delay offsets were calibrated using either recorded phase calibration tones or by fringe fitting a strong calibration source and applying the resulting delay corrections to all scans. This aligned phases within the four 16-MHz-wide IF bands. All data were examined for discrepant values or interference, and to verify that the *a priori* calibration had been applied correctly.

4.2. Ionosphere Delay Calibration

Our observations did not include very widely separated frequency bands, so the dispersive ionosphere delay (and Faraday rotation) was calibrated using global maps of zenith total electron content (TEC) determined from GPS networks at two-hour intervals. Linear interpolation between global TEC maps bracketing an observation was used, including a longitude correction to account for the fact that the ionosphere should be approximately fixed with respect to the Sun, not the Earth.

4.3. Troposphere Delay Calibration

Multi-band delays were calculated for a sample of ~ 15 strong sources observed in a rapid sequence over a wide range of elevation angles. A linear fit to the four IF phases was used to determine the multi-band delay for each source. At least three IFs were required to have good data. Zenith troposphere delays and clock errors (offsets and rates) were fit to the measured multi-band delays using the Chao (1974) mapping function (see Sovers et al. (1998); Mioduszewski & Kogan (2004)). This calibration removed the residual tropospheric delay, thus aligning the phases between all four IF bands.

Figure 3 shows the improvement in image quality produced by this manual troposphere delay calibration. Note that the correction is mainly in the declination direction, as would be expected for a low declination source. The position offset is about 0.2 mas, corresponding to a difference in differential delay of a few mm on the longer VLBA baselines. Seven of the eight epochs reported in this paper were improved in this way. However, for one epoch (BJ061D) all attempts to calibrate troposphere delays manually produced poorer results, and we relied on the basic correlator troposphere model for this epoch.

4.4. Bandpass Calibration

A strong calibration source was observed during each epoch to determine any remaining antenna-based delays and to calibrate the bandpass response. After this step, scan-averaged phases were inspected for all calibration sources and baseline to verify that the phases were constant with

Table 2. Observing Epochs and Phase Reference Sources

Epoch	Date	Reference Source	Angular Separation (deg)	Flux Density (Jy)
BJ061A	2006 Oct	J0931+1414	2.5	0.15
BJ061B	2007 Mar	J0931+1414	< 2	0.15
BJ061C	2007 Jun	J0931+1414	< 2	0.15
BJ061D	2008 Jan	J1025+1253	3.5	0.23
BJ061E	2008 Jun	J1025+1253	~ 1	0.23
BJ061F	2008 Aug	J1025+1253	< 3	0.23
BJ061G	2008 Nov	J1127+0555	< 0.5	0.10
BJ061H	2009 Apr	J1112+0724	< 0.5	0.20

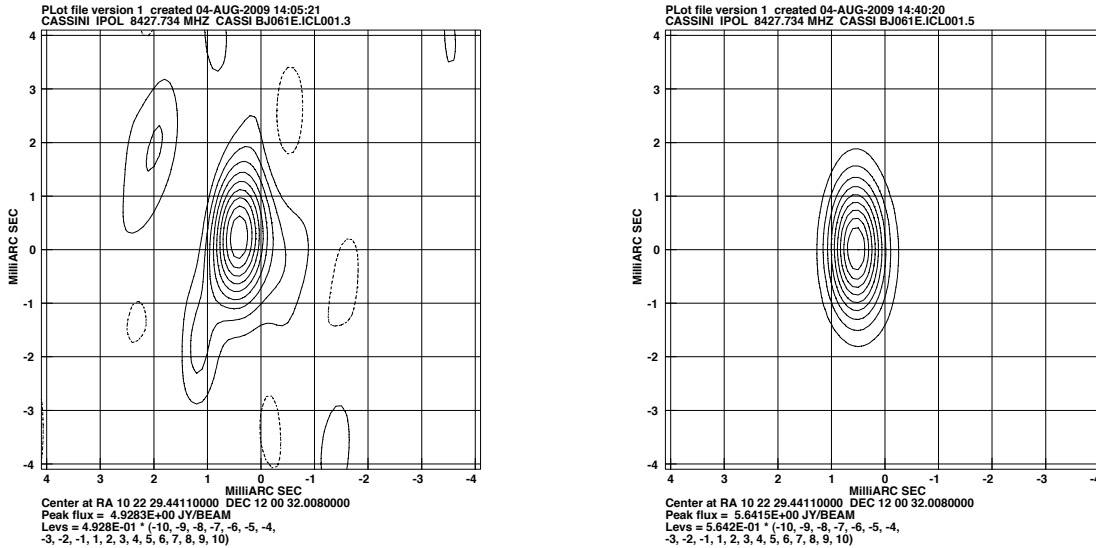


Fig. 3.— Effect of manual troposphere delay calibration. The left panel is the phase-referenced Cassini image from epoch 5 without troposphere calibration. The right panel shows the improvement when troposphere delays were estimated for each antenna using calibrators observed over a wide range of elevation angles. Note the reduction in scattered power and the higher peak flux density (4.93 Jy/beam on left, 5.64 Jy/beam on right). Note also the small shift in declination between the two images.

frequency within and between IF bands.

4.5. Phase-Referenced Imaging

Self-calibration with a point source model was used to optimize the phases of the phase reference calibrator, and then these phases were applied to the Cassini visibilities. No self-calibration was applied to the Cassini data. At this state images were made of both the phase reference source and Cassini. The phase reference source, by self-calibration, was always located at its *a priori* sky position. We used the phase calibrator image to verify that a point source model was adequate.

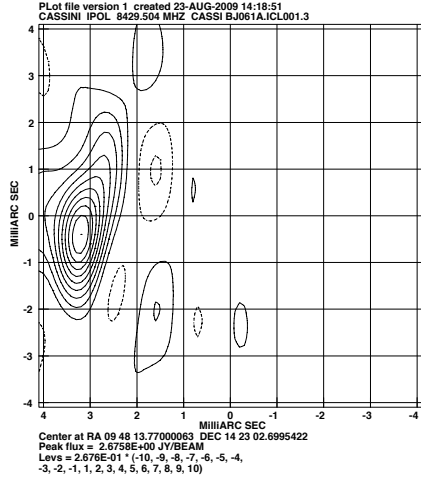
The location of the peak signal in the Cassini image was measured with the AIPS task maxfit and used to shift the image to place Cassini at (or very near) the phase center. Two-dimensional quadratic fits to the peaks in images of Cassini provide positions relative to the nominal phase center with formal errors under 0.02 mas in both coordinates, far smaller than our systematic errors. The post-shift baseline phases were examined to verify that the removal of the position offset had centered the Cassini signal at the *a priori* position.

Figures 4 and 5 show the unshifted images of Cassini for all eight epochs. The first four epochs, in Figure 4, all have large offsets from the phase center. This was caused by a one-second error in the time used when calculating the spacecraft position during correlation, the result of ignoring a leap second. This error was discovered in 2008 March, but re-correlation with a corrected correlator model was not possible because the raw data recordings were no longer available. The total delays were unaffected by this offset. The last four epochs, in Figure 5, show much smaller position offsets after the leap second error was found and corrected.

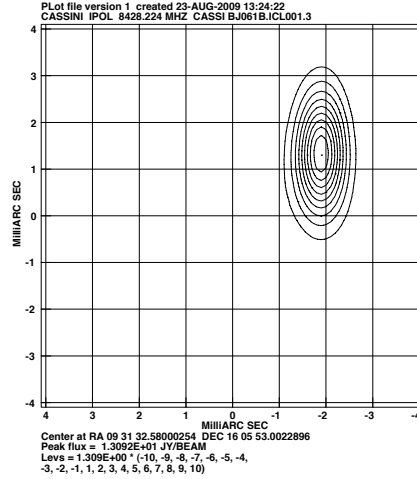
4.6. Phase Reference Source Positions

The position of the peak Cassini signal was measured with respect to its image phase center, which in turn depended on the assumed position of the phase reference source and the geometric model. Thus, any error in the phase reference source position produces a corresponding error in the position of Cassini. We used the best available *a priori* positions for our phase reference sources during data analysis, but improved positions have recently become available as part of the ICRF2 catalog (Fey et al. 2009).

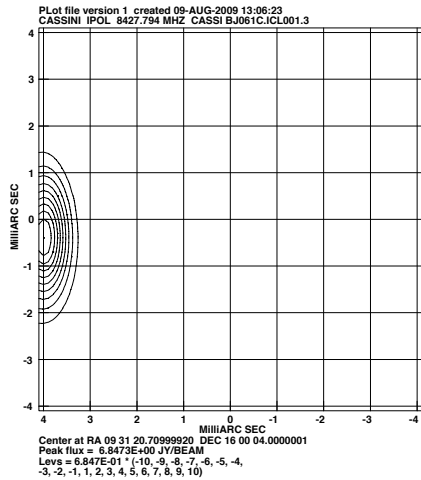
Table 3 shows the ICRF2 position of our primary phase reference sources. The maximum difference between our *a priori* reference source positions and the ICRF2 positions is 0.16 mas (for J0931+1414 in right ascension); all other position differences are less than 0.1 mas. Note, however, that the ICRF2 position errors vary by more than an order of magnitude between sources. Future observations will continue to improve the less accurate source positions.



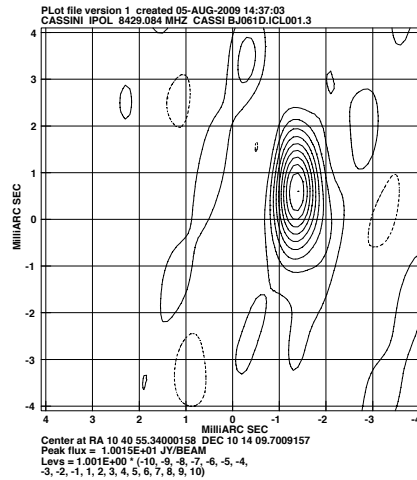
(a) Epoch BJ061A



(b) Epoch BJ061B

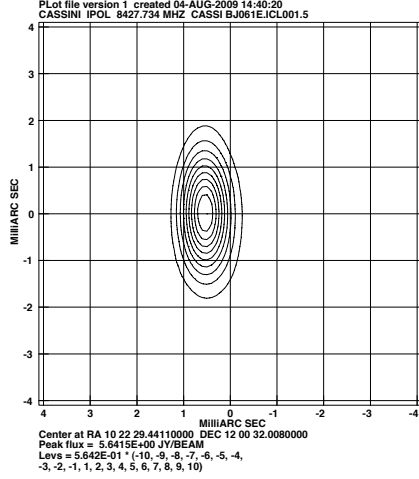


(c) Epoch BJ061C

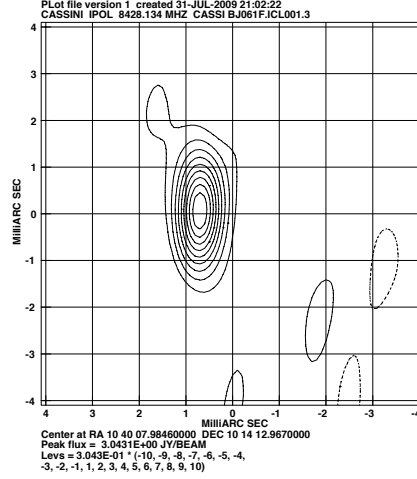


(d) Epoch BJ061D

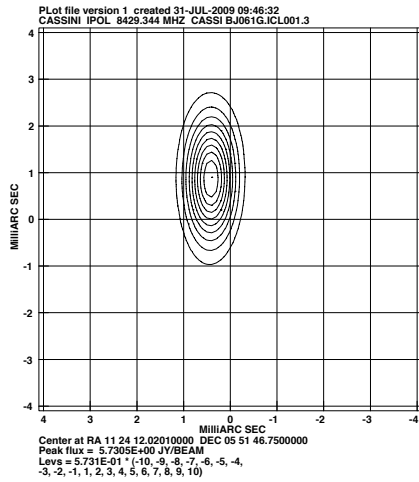
Fig. 4.— Phase-referenced images of Cassini from the first four epochs. The large and variable position offsets are caused by a one-second error in the spacecraft orbit calculations. The peak flux densities are 2.68 Jy/beam (upper left), 13.09 Jy/beam (upper right), 6.85 Jy/beam (lower left), and 10.02 Jy/beam (lower right). In all cases the contour levels are -20, -10, 10, 20, 30, 40, 50, 60, 70, 80, and 90% of the peak flux density.



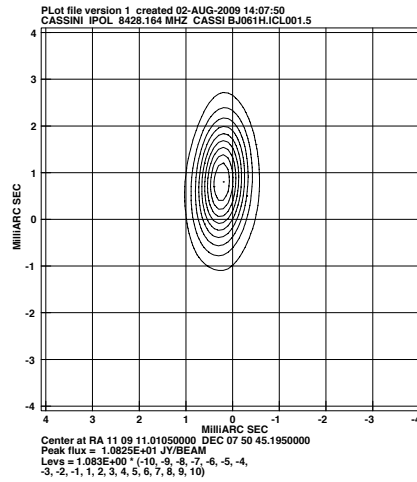
(a) Epoch BJ061E



(b) Epoch BJ061F



(c) Epoch BJ061G



(d) Epoch BJ061H

Fig. 5.— Phase-referenced images of Cassini from the last four epochs. The peak flux densities are 5.64 Jy/beam (upper left), 3.04 Jy/beam (upper right), 5.73 Jy/beam (lower left), and 10.83 Jy/beam (lower right). In all cases the contour levels are -20, -10, 10, 20, 30, 40, 50, 60, 70, 80, and 90% of the peak flux density.

A recurring issue in radio astrometry is the positional stability of the radio cores used to define the ICRF and for narrow-angle phase referenced measurements. VLBI group delays give the position of the base of a radio jet, while VLBI phase delays give a frequency-dependent offset from the group delay position because of frequency-dependent opacity along the jet. The ICRF is based on group delay measurements, and thus is relatively insensitive to jet opacity effects. Our phase referenced astrometric measurements of Cassini, however, are directly affected by any variations in the apparent centroid position of our phase reference sources.

Phase and group delay positions are typically offset by 0.17 mas at 8.4 GHz (Porcas 2009). This offset is comparable to tropospheric calibration errors, and errors in the ICRF/ICRF2 positions of individual sources in many cases.

4.7. Total Delays

The geometric model, including *a priori* antenna and source positions and the measured delays, plus the residual delay from the antenna phases determined from the shifted Cassini image, were output from AIPS in a series of tables. These tables were text listings of the AN (antenna geometry), SU (source geometry), CL (correlator model and image position shift), and SN (residual phases) calibration tables associated with a visibility data file AIPS. They were used to generate total delay values that could be used by JPL navigation software.

Figure 6 shows an example of the observed total delays for Cassini and the phase reference source on one baseline, and the difference in total delays between the sources based on interpolation to identical times. The variation in differential delay during an observing epoch defines the angular offset between Cassini and the phase reference source.

Table 3. Primary Phase Reference Sources

Source	RA (J2000)	DEC (J2000)
J0931+1414	09 ^h 31 ^m 05 ^s .342445 ±0 ^s .000029	14°14'16.51897"±0.00090"
J1025+1253	10 ^h 25 ^m 56 ^s .285370 ±0 ^s .000004	12°53'49.02201"±0.00008"
J1112+0724	11 ^h 12 ^m 09 ^s .558539 ±0 ^s .000016	07°24'49.11804"±0.00050"
J1127+0555	11 ^h 27 ^m 36 ^s .525564 ±0 ^s .000066	05°55'32.05999"±0.00172"

Note. — Positions and errors are from Fey et al. (2009).

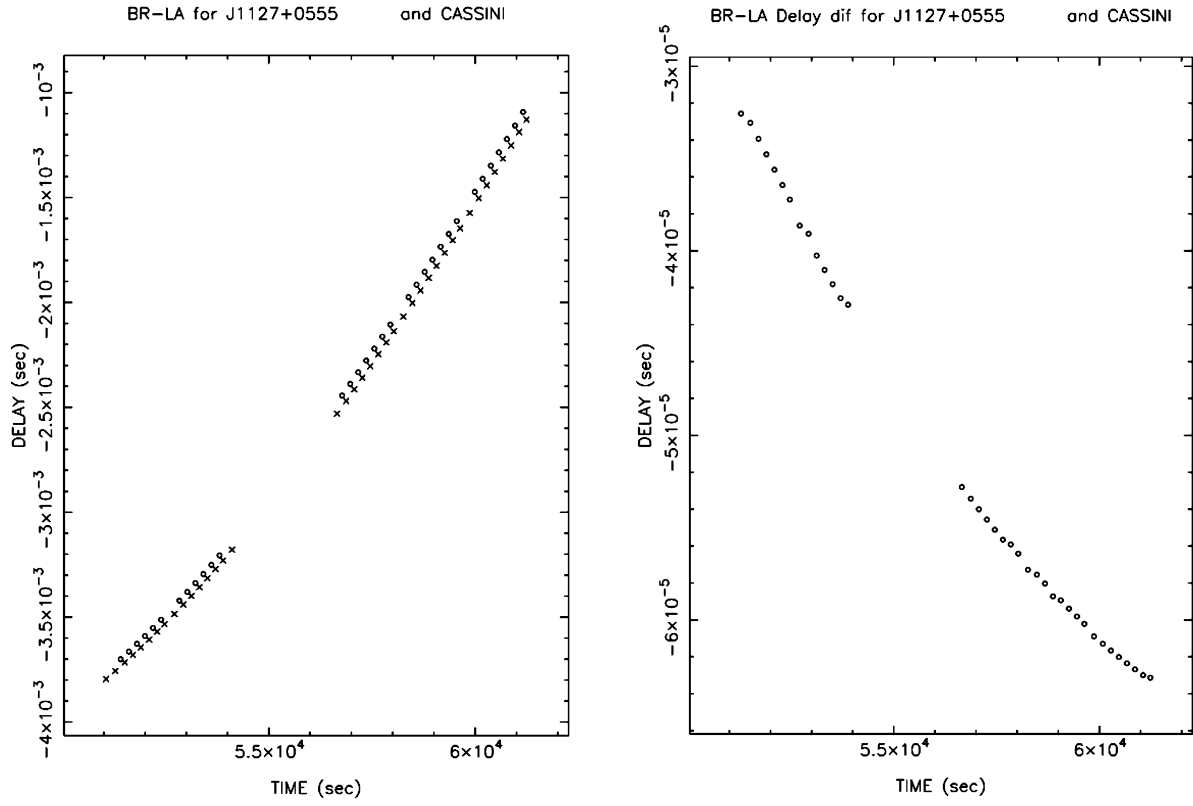


Fig. 6.— Example of total delays on one baselines for Cassini and the phase reference source (left), and the differential delays between the two sources (right). The horizontal axis spans approximately four hours of time.

5. Results

Table 4 lists our results from phase-referenced imaging of Cassini during VLBA observing epochs from October 2006 to April 2009. (Preliminary versions of these results were reported in Jones et al. 2009a; 2009b.) The estimated measurement errors, including residual systematic errors from troposphere delay calibration and reference sources positions, are ± 0.2 mas in right ascension and ± 0.4 mas in declination. The errors are larger in declination because of the low declination of Saturn/Cassini, which foreshortens the north-south angular resolution of the VLBA. The two left columns show Cassini image position offsets that have been corrected for the one-second time error that occurred during our first four epochs. This correction was made by subtracting an angle corresponding to the spacecraft proper motion during one second of time from each measured coordinate offset.

There is marginal evidence for a small position offset in right ascension ($+0.39 \pm 0.12$ mas). It is important to see if future epochs continue to show this offset. Given the sometimes large uncertainties in the ICRF positions of our phase reference sources, this offset is not currently significant. There is no significant evidence for a systematic position offset in declination at this time ($+0.47 \pm 0.30$ mas). The errors quoted here are from the scatter in the measured offsets; they do not include the individual offset measurement errors or the reference source position errors. If we consider only the three epochs that used J1025+1253, the reference source with the most accurate ICRF position, the conclusion is unchanged. However, additional epochs and improved phase reference source positions are needed to verify the reality of any right ascension offset.

Table 5 lists the positions of the Cassini spacecraft determined from the VLBA total delay measurements, analyzed at JPL. This table includes two additional epochs from VLBA experiment BR103 in 2004, and an epoch in 2009 February from Fomalont et al. (2010). We included data from the 2004 and 2009 February observations because they used the same observing technique and instrumentation to determine astrometric positions for Cassini as the BJ061 experiments used.

Figure 7 shows a comparison of the residual delays on one baseline (BR-FD) from one epoch (February 2009), illustrating the level of consistency between the two data analysis paths. The differences are ~ 2 ps, which is comparable to the numerical precision expected from interpolating the planetary ephemeris for Saturn. (The JPL ephemeris is integrated in quadruple precision, but the results are stored in double precision so the numerical noise in the ~ 5000 light second distance to Saturn is a few ps.) The overall slope from about -5 ps to $+5$ ps during this epoch corresponds to the residual Cassini position offset from the *a priori* position, and is clearly seen equally in the delays from both analyses.

Table 4. Cassini Position Offsets from Phase-Reference Images

Epoch Label	Observing Date	Image RA Offset (mas)	Image DEC Offset (mas)	Corrected RA Offset (mas)	Corrected DEC Offset (mas)
BJ061A	2006 Oct	+3.0	−0.4	+0.5	+0.3
BJ061B	2007 Mar	−2.1	+1.3	+0.4	+0.5
BJ061C	2007 Jun	+3.8	−0.4	+0.4	+0.7
BJ061D	2008 Jan	−1.5	+0.6	+0.2	−0.2
BJ061E	2008 Jun	+0.4	+0.0	+0.4	+0.0
BJ061F	2008 Aug	+0.6	+0.0	+0.6	+0.0
BJ061G	2008 Nov	+0.3	+0.9	+0.3	+0.9
BJ061H	2009 Apr	+0.2	+0.8	+0.3	+0.8

Table 5. Observed Cassini Positions in ICRF 2.0 Reference Frame

Date	Time (UTC)	Observed Right Ascension	Observed Declination
2004 Sep 08	18:00:00	07 ^h 45 ^m 26 ^s .89383	+21°02′15.0413″
2004 Oct 20	14:00:00	07 ^h 56 ^m 26 ^s .30351	+20°38′57.4360″
2006 Oct 11	17:00:00	09 ^h 39 ^m 57 ^s .36913	+14°57′22.1298″
2007 Mar 01	07:00:00	09 ^h 31 ^m 30 ^s .71957	+16°06′01.4992″
2007 Jun 08	00:00:00	09 ^h 31 ^m 22 ^s .39987	+15°59′55.8154″
2008 Jan 12	10:00:00	10 ^h 40 ^m 54 ^s .92717	+10°14′12.4080″
2008 Jun 14	00:00:00	10 ^h 22 ^m 29 ^s .45360	+12°00′31.9588″
2008 Aug 01	22:00:00	10 ^h 40 ^m 09 ^s .03733	+10°14′07.3040″
2008 Nov 11	17:00:00	11 ^h 24 ^m 12 ^s .79125	+05°51′44.0929″
2009 Feb 11	14:00:00	11 ^h 27 ^m 09 ^s .89646	+05°58′57.6093″
2009 Apr 24	06:00:00	11 ^h 09 ^m 09 ^s .77073	+07°50′58.7079″

Note. — Positions are geocentric at the listed observation times.

The derived J2000 (ICRF 2.0) positions of the Saturn system barycenter from VLBA observations of Cassini, including detailed Cassini orbit reconstructions, are listed in Table 6. This table is the primary result of our observations. The Cassini orbital trajectory is produced by numerical integration of the equations of motion as part of a global Saturn ephemeris and gravity field solution (e.g., Antreasian et al. (2006); Jacobson et al. (2006)). These solutions include a large number of historical and recent observations. The equations of motion for Cassini include Newtonian accelerations due to the Sun, planets, and the Saturnian satellites, relativistic perturbations due to the Sun, Jupiter, and Saturn, and perturbations due to the oblateness of Saturn. Non-gravitational forces such as attitude control and trajectory correction maneuvers and solar radiation pressure are also modeled. Saturn’s satellite dynamics include the mutual interactions of the satellites and perturbations due to the Sun, Jupiter, Uranus, Neptune, and Saturn’s oblateness.

Table 7 gives the post-fit residuals for each epoch in Table 6 with respect to the DE422 ephemeris, which was fit to the VLBA data. For comparison, residuals are also give with respect to the widely used DE405 ephemeris.

The observed positions of the Saturn barycenter with respect to the DE422 planetary ephemeris are shown in Figure 8. The DE422 ephemeris is the result of fitting the DE421 ephemeris (Folkner, Williams, & Boggs (2008); Folkner, Williams, & Boggs (2009)) to the new Cassini VLBA data, along with about 18 months of additional tracking data from Venus Express, Mars Reconnaissance Orbiter, Mars Express, Mars Odyssey, and CCD observations of the outer planets. Errors are estimated independently by the ephemeris fitting program used at JPL, and include uncertainties in both the VLBA measurements and the position of Cassini with respect to the Saturn barycenter. The weighted mean offset after fitting is less than 0.2 mas in right ascension and 0.3 mas in declination, consistent with the expected uncertainties.

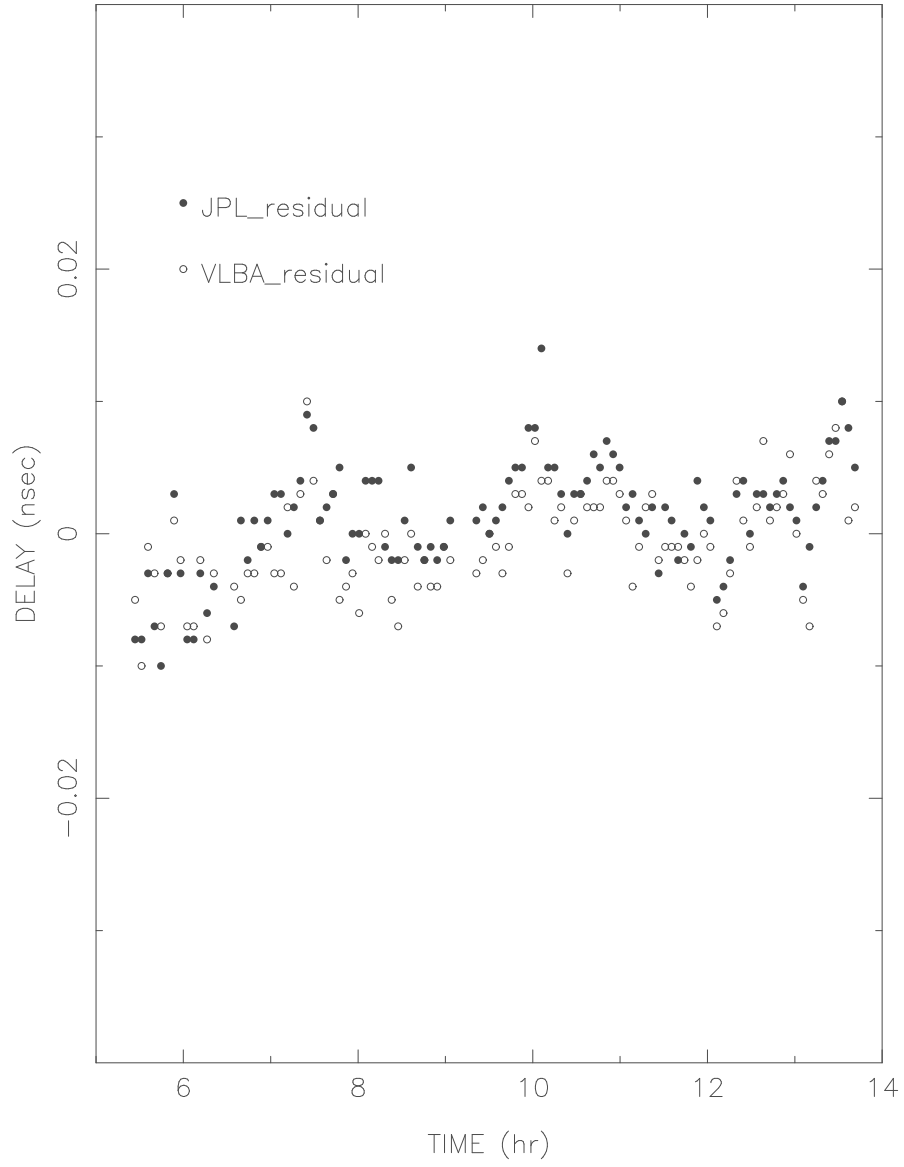


Fig. 7.— Residual delays from the JPL analysis of VLBA total delay data and delays determined from phase referenced imaging of Cassini.

Table 6. Observed Saturn Barycenter Positions in ICRF 2.0 Reference Frame

Date	Time (UTC)	Observed Right Ascension	Observed Declination	Error in R.A. (s)	Error in Dec. (")
2004 Sep 08	18:00:00	07 ^h 43 ^m 57 ^s .853974	+21°06′11.47431″	0.000073	0.00052
2004 Oct 20	14:00:00	07 ^h 55 ^m 52 ^s .671888	+20°38′20.56188″	0.000006	0.00020
2006 Oct 11	17:00:00	09 ^h 39 ^m 54 ^s .457150	+14°57′55.39349″	0.000033	0.00113
2007 Mar 1	07:00:00	09 ^h 31 ^m 40 ^s .709327	+16°02′49.54177″	0.000029	0.00091
2007 Jun 08	00:00:00	09 ^h 31 ^m 40 ^s .531553	+15°59′06.93823″	0.000029	0.00094
2008 Jan 12	10:00:00	10 ^h 41 ^m 00 ^s .869116	+10°11′45.98652″	0.000010	0.00031
2008 Jun 14	00:00:00	10 ^h 22 ^m 29 ^s .258227	+11°59′01.78134″	0.000007	0.00028
2008 Aug 01	22:00:00	10 ^h 40 ^m 07 ^s .840686	+10°12′49.68886″	0.000009	0.00022
2008 Nov 11	17:00:00	11 ^h 24 ^m 07 ^s .553645	+05°51′34.99358″	0.000065	0.00173
2009 Feb 11	14:00:00	11 ^h 27 ^m 15 ^s .292877	+05°56′37.40025″	0.000016	0.00051
2009 Apr 24	06:00:00	11 ^h 09 ^m 02 ^s .825609	+07°52′58.01128″	0.000017	0.00053

Note. — Positions are geocentric at the listed signal reception times. These define the direction vector from the Earth geocenter at signal reception time to Saturn’s position at signal transmission time (earlier than signal reception by the light travel time from Saturn). Thus, no aberration or relativistic light deflection has been applied.

Table 7. VLBA Position Residuals for Saturn Barycenter

Date	Time (TDB)	α -DE422 ($''$)	δ -DE422 ($''$)	α -DE405 ($''$)	δ -DE405 ($''$)
2004 Sep 08	18:00:00	-0.00181	-0.00029	0.11810	-0.04001
2004 Oct 20	14:00:00	-0.00004	0.00012	0.12933	-0.04415
2006 Oct 11	17:00:00	0.00013	-0.00007	0.13055	-0.04509
2007 Mar 1	07:00:00	0.00010	0.00002	0.15703	-0.04761
2007 Jun 08	00:00:00	0.00024	0.00008	0.13570	-0.03817
2008 Jan 12	10:00:00	0.00005	-0.00001	0.14914	-0.04794
2008 Jun 14	00:00:00	0.00007	-0.00005	0.13594	-0.03678
2008 Aug 01	22:00:00	0.00002	-0.00010	0.12708	-0.03553
2008 Nov 11	17:00:00	0.00005	0.00080	0.12868	-0.03666
2009 Feb 11	14:00:00	-0.00006	0.00024	0.14930	-0.04090
2009 Apr 24	06:00:00	-0.00005	0.00045	0.14785	-0.03653

Note. — TDB = Barycentric Dynamic Time, a general relativistic coordinate time centered on the solar system barycenter.

6. Conclusions

We have demonstrated repeatable phase referenced astrometry of the Cassini spacecraft using the VLBA, and verified consistent position determinations from direct imaging and from total delay measurements. Future observations will increase the time span of accurate position measurements, leading to ever improving constraints on the planetary ephemeris. In addition, continuing improvement in the accuracy of phase reference source positions will allow a more accurate tie of our Cassini positions to the ICRF.

The Cassini mission has recently been extended until 2017, with further extensions likely in the future. By extending our VLBI observations beyond 2012 we will have high accuracy measurements over more than a quarter of Saturn’s orbital period. The error in determining the plane of Saturn’s orbit (latitude) decreases rapidly as the time span of observations approaches 1/4 of the orbital period. The error in longitude decreases approximately linearly with time span.

The next mission to the outer planets will be the JUNO mission to Jupiter. This orbiting mission will provide an opportunity to use the same phase referenced astrometry techniques with the VLBA, and thereby improve the ephemeris of Jupiter in a similar manner.

We are grateful to Larry Teitelbaum for support of this project through the Advanced Tracking and Observational Techniques office of JPL’s Interplanetary Network Directorate, and to John Benson and the VLBA operations staff at NRAO for their excellent support of these observations. We also thank Peter Antreasian and Fred Pelletier at JPL for providing the reconstructed Cassini orbit files used for data correlation at NRAO. The anonymous referee’s comments led to significant improvements in the paper. The VLBA is a facility of the National Radio Astronomy Observatory, which is operated by Associated Universities, Inc., under a cooperative agreement with the National Science Foundation. Part of this research was carried out at the Jet Propulsion Laboratory, California Institute of Technology, under contract with the National Aeronautics and Space Administration.

Facilities: VLBA.

REFERENCES

- Antreasian, P. G., Bordi, J. J., Criddle, K. E., Ionasescu, R. A., Jacobson, R. A., & Jones, J. B., 2006, AIAA/AAS Astrodynamics Specialist Conference and Exhibit (Keystone, CO), paper 2006-6400
- Antreasian, P. G., Ardalan, S. M., Beswich, R. M., Criddle, K. E., Ionasescu, R., Jacobson, R. A., Jones, J. B., MacKenzie, R. A., Parcher, D. W., Pelletier, F. J., Roth, D. C., Thompson, P. F., & Vaughan, A. T., 2008, SpaceOps Conf. (ESA/EUMETSAT/AIAA), paper AIAA 2008-3433

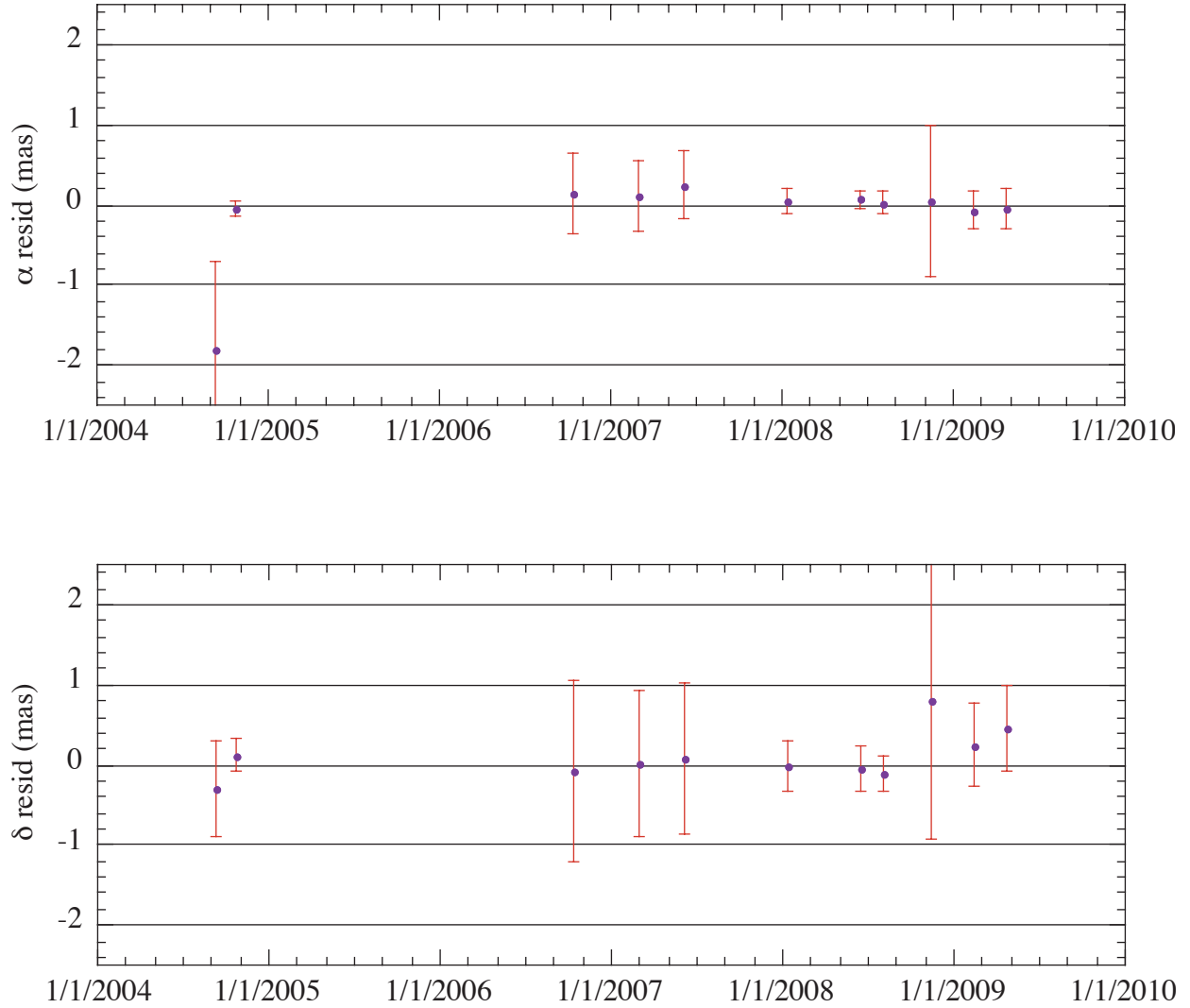


Fig. 8.— Saturn positions based on VLBA data compared to the DE422 JPL Saturn ephemeris positions. The error estimates include expected uncertainties in the phase reference source positions prior to our improved tie of these sources to the ICRF, and also include errors in the solutions for the Cassini orbit about Saturn. The first two data points were obtained by a separate observing program; the first data point was obtained prior to Cassini orbit insertion at Saturn.

- Campbell, D. B., Chandler, J. F., Ostro, S. J., Pettengill, G. H., & Shapiro, I. I., 1978, *Icarus*, 34, 254
- Chao, C. C., 1974, JPL Tech. Report, 32-1587, 61
- Duxbury, T. C., & Callahan, J. D., 1989, *A&A*, 216, 284
- Fey, A.L., Ma, C., Arias, E.F., Charlot, P., Feissel-Vernier, M., Gontier, A.-M., Jacobs, C.S., Li, J., & MacMillian, D.S., 2004, *AJ*, 127, 3587
- Fey, A. L., Gordon, D. & Jacobs, C. S. (eds.), 2009, IERS Technical Note No. 35, International Earth Rotation and Reference Systems Service, <http://www.iers.org/MainDisp.csl?pid=46-1100252>
- Folkner, W. M., Williams, J. G., & Boggs, D. H., JPL Memorandum, 343R-08-003, 20
- Folkner, W. M., Williams, J. G., & Boggs, D. H., 2009, JPL Interplanetary Network Progress Report, 42-178 (August 15, 2009)
- Fomalont, E. B., & Kopeikin, S. M., 2003, *ApJ*, 598, 704
- Fomalont, E., & Kogan, L., 2005, AIPS Memo, 111, (<http://www.aips.nrao.edu/aipsdoc/html>)
- Fomalont, E., 2006, IVS 2006 General Meeting Proc., 307 (<http://ivscc.gsfc.nasa.gov/publications/gm2006/fomalont>)
- Fomalont, E., Kopeikin, E., Jones, D., Honma, M., & Titov, O., 2010, *Relativity in Fundamental Astronomy: Dynamics, Reference Frames, and Data Analysis*, ed. S. Klioner, P.K. Seidelmann, & M. Soffel (IAU Symp. 261, Cambridge Univ. Press), 291
- Guirado, J. C., Reynolds, J. E., Lestrade, J.-F., Preston, R. A., Jauncey, D. L., Jones, D. L., Tzioumis, A. K., Ferris, R. H., King, E. A., Lovell, J. E. J., McCulloch, P. M., Johnston, K. J., Kingham, K. A., Martin, J. O., White, G. L., Jones, P. A., Arenou, F., Froeschle, M., Kovalevsky, J., Martin, C., Lindegren, L., & Soderhjelm, S., 1997, *ApJ*, 490, 835
- Guirado, J. C., Ros, E., Jones, D. L., Lestrade, J.-F., Marcaide, J. M., Perez-Torres, M. A., & Preston, R. A., 2001, *A&A*, 371, 766
- IAU Transactions, vol. XXVIIA, Reports on Astronomy 2006-2009, ed. K A. van der Hucht (Cambridge Univ. Press), Commission 4 Triennial Report, 5
- Jacobson, R. A., Haw, R. J., McElrath, T. P., & Antreasian, P. G., 1999, AAS/AIAA Conf., paper AAS 99-330
- Jacobson, R. A., Antreasian, P. G., Bordi, J. J., Criddle, K. E., Ionasescu, R., Jones, J. B., Mackenzie, R. A., Meek, M. C., Parcher, D., Pelletier, F. J., Owen, W. M., Jr., Roth, D. C., Roundhill, I. M., & Stauch, J. R., 2006, *AJ*, 132, 2520

- Jones, D., Fomalont, E., Dhawan, V., Romney, J., Lanyi, G., & Border, J., 2009a, *BAAS*, 41, 189 (paper 401.06)
- Jones, D., Fomalont, E., Dhawan, V., Romney, J., Lanyi, G., & Border, J., 2009b, *Proc. National Radio Science Meeting (Boulder: URSI)*, J5-1
- Lanyi, G., Border, J., Benson, Dhawan, V., Fomalont, E., Martin-Mur, T., McElrath, T., Romney, J., & Walker, C., 2005, *JPL Interplanetary Network Progress Report*, 42-162
- Lanyi, G., Bagri, D. S., & Border, J. S., 2007, *Proc. IEEE*, 95, 2193
- Lestrade, J.-F., Rogers, A. E. E., Whitney, A. R., Niell, A. E., Phillips, R. B., & Preston, R. A., 1990, *AJ*, 99, 1663
- Lestrade, J.-F., Preston, R. A., Jones, D. L., Phillips, R. B., Rogers, A. E. E., Titus, M. A., Rioja, M. J., & Gabuzda, D. C., 1999, *A&A*, 344, 1014
- Lestrade, J.-F., 2004, *The Role of VLBI in Astrophysics, Astrometry and Geodesy*, ed. F. Mantovani & A. Kus (Kluwer), 383
- Ma, C., et al., 1998, *AJ*, 116, 516
- Mioduszewski, A. J., & Kogan, L., 2004, *AIPS Memo 110* (www.aips.nrao.edu/aipsdoc.html)
- Muhleman, D. O., Berge, G. L., & Rudy, D. J., 1985, *Celestial Mech.*, 37, 329
- Muhleman, D. O., Berge, G. L., Rudy, D. J., & Niell, A. E., 1986, *AJ*, 92, 1428
- Porcas, R. W., 2009, *A&A*, 505, L1
- Romney, J. D., 1999, *Synthesis Imaging in Radio Astronomy II*, ed. G. B. Taylor, C. L. Carilli, & R. A. Perley (San Francisco: ASP), 57
- Sovers, O. J., Fanelow, J. L. & Jacobs, C. S., 1998, *Rev. Mod. Phys.*, 70, 1393
- Standish, E. M., 2004, *A&A*, 417, 1165
- Standish, E. M., 2006, *JPL Interoffice Memorandum*, 343R-06-005, 1 May 2006
- Verbiest, J. P. W., Bailes, M., van Straten, W., Hobbs, G. B., Edwards, R. T., Manchester, R. N., Bhat, N. D. R., Sarkissian, J. M., Jacoby, B. A., & Kulkarni, S. R., 2008, *ApJ*, 679, 675